Table S1 Comparison of density and diffusion coefficient of solvents computed from classical MD simulations with previous literature results.

| **Solvents** | **Density ($g/cm^3$) Simulation T=298 K** | **Density ($g/cm^3$) Experimental T=298 K** | **Diffusion Coefficient*10^-11 ($m^2/s$) Simulation T=298 K** | **Diffusion Coefficient*10^-11 ($m^2/s$) Experimental T=298 K** |
|---|---|---|---|---|
| AN | 0.7904 | 0.777(±2)[5] | 350.28((±2.3) | 420[5] |
| THF | 0.889 | 0.8823[6] | 211.34(±19.2) | 300[7] |
| DMSO | 1.106 | 1.096[6] | 89.92(±4.69) | 83.0[8] |
| G1 | 0.851 | 0.86114[9] | 230(±4.85) @ 303K | 315 @ 303K[7] |
| G2 | 0.942 | 0.93883[9] | 70.4(±4.2) @303K | 130@303K[7] |
| G4 | 1.025 | 1.007[10] | 8.34(±1.8) @ 312K | 11.34 @ 312 K |
| DMA | 0.676 | 0.65[11] | 480(±23) | ~550[12] |

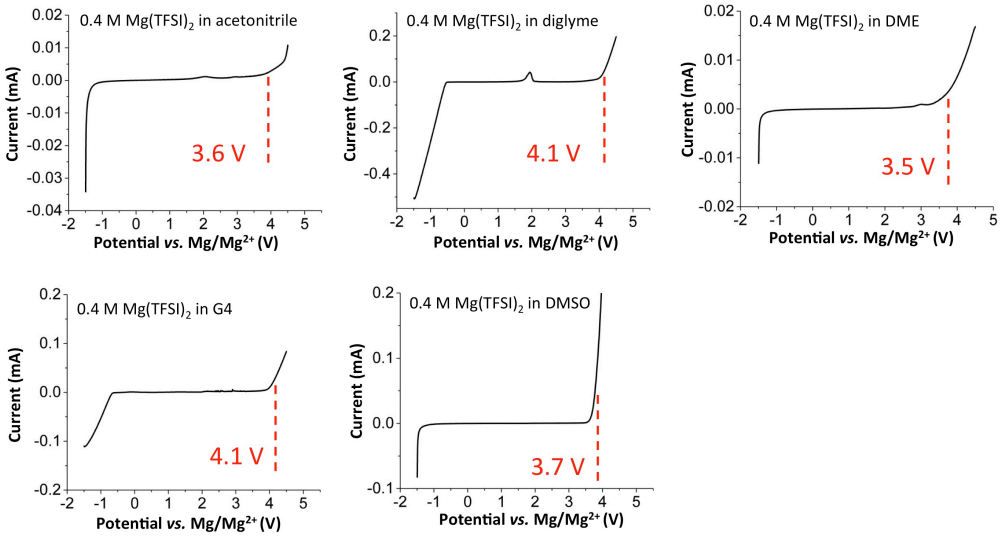


Figure S1. Linear sweep voltammetry measurement for the MgTFSI in various solvent including acetonitrile, G1, G2, G4 and DMSO. The electrolyte concentration was kept as 0.4M. The sweep rate was kept as 25 V/sec. Three electrodes configuration is used with Pt disk as working electrode, Mg ribbon as counter and reference electrode. MgTFSI exhibits stability for up to 4V in most of the solvents.

Table S2. Comparison of experimental measurements and theoretical predictions of anodic and cathodic potential limits, employing both combined explicit-implicit as well as implicit solvent models for the salt anion electrochemical stability window. For the experimental values, the anodic limit is interpreted as the lower limit of oxidation potential for the anion, as the current could originate from other decomposing species. In the combined explicit-implicit model, one solvent molecule is coordinated with the anion, and the IEF-PCM model is employed to capture solvents effect at longer distances. As observed in the table, the trends obtained from the implicit solvent model result correlate well with the combined explicit-implicit model results as well as experimental values while reporting generally wider electrochemical windows.

| **Solvents** | **Combined Explicit-Implicit model (V vs $Mg/Mg^{2+}$)** | | **Implicit model (V vs $Mg/Mg^{2+}$)** | | **Experimental anion anodic stability and source (V vs $Mg/Mg^{2+}$)** |
|---|---|---|---|---|---|
| | IP | EA | IP | EA | |
| **TFSI in Acetonitrile** | 5.08 | -1.57 | 5.13 | -1.47 | >3.6 This work |
| **TFSI in Diglyme** | 4.37 | -2.02 | 4.93 | -2.05 | >4.1 This work<br>>4.0[1] |
| **TFSI in DMSO** | 5.13 | -1.52 | 5.14 | -1.44 | >3.7 This work |
| **TFSI in THF** | 4.87 | -2.11 | 4.94 | -2.01 | |
| **TFSI in DME** | | | 4.93 | -2.05 | >3.5 This work<br>>4.0[1] |
| **TFSI in G4** | | | 4.95 | -1.99 | >4.1 This work |
| **$BH_4$ in THF** | | | 3.43 | -3.08 | >2.3[2]<br>>2.0[3] |
| **$BF_4$ in Acetonitrile** | | | 7.39 | -1.74 | >5.3[4] |

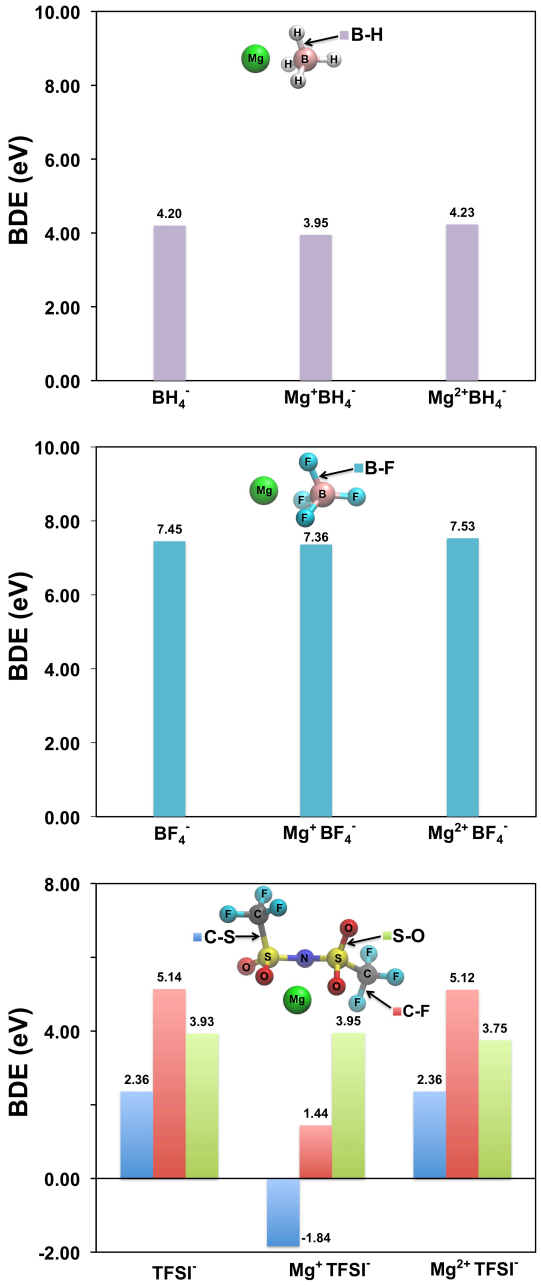


Figure S2. Bond Dissociation Energy (BDE) of $BH_4^-$, $BF_4^-$, and $TFSI^-$ in different chemical environments corresponding to well-solvated, $Mg^+$ ion-paired and $Mg^{2+}$ ion-paired configurations using the combined solvent model with one explicit solvent molecule and PCM.

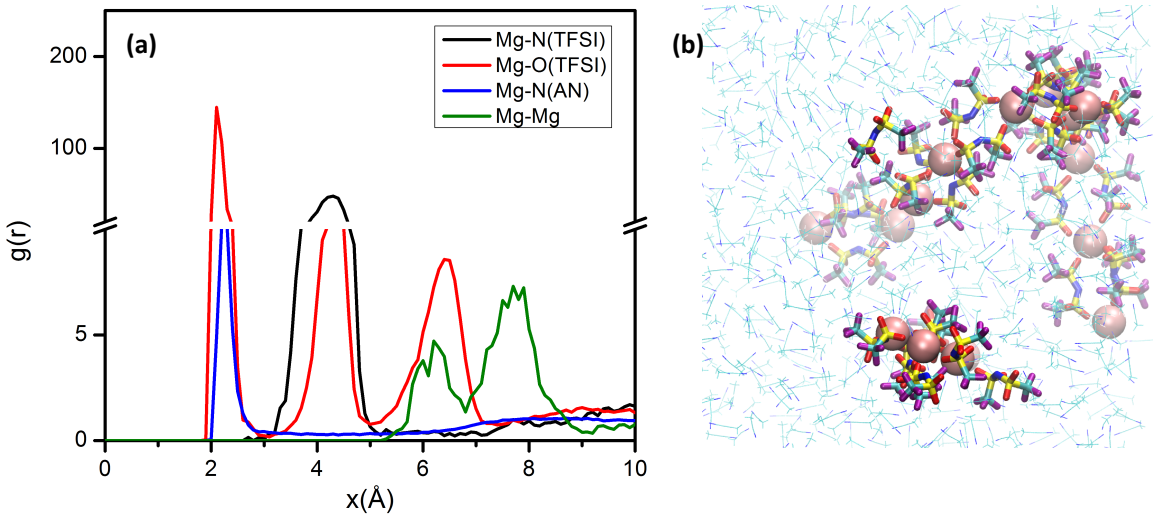


Figure S3. (a) Radial distribution function of Mg-N(TFSI), Mg-O(TFSI), Mg-N(AN) and Mg-Mg (b) representative simulation snapshot of 0.4 M $Mg(TFSI)_2$ in AN at 298 K. Mg depicted in pink in space-filling format, TFSI in licorice and AN in line format

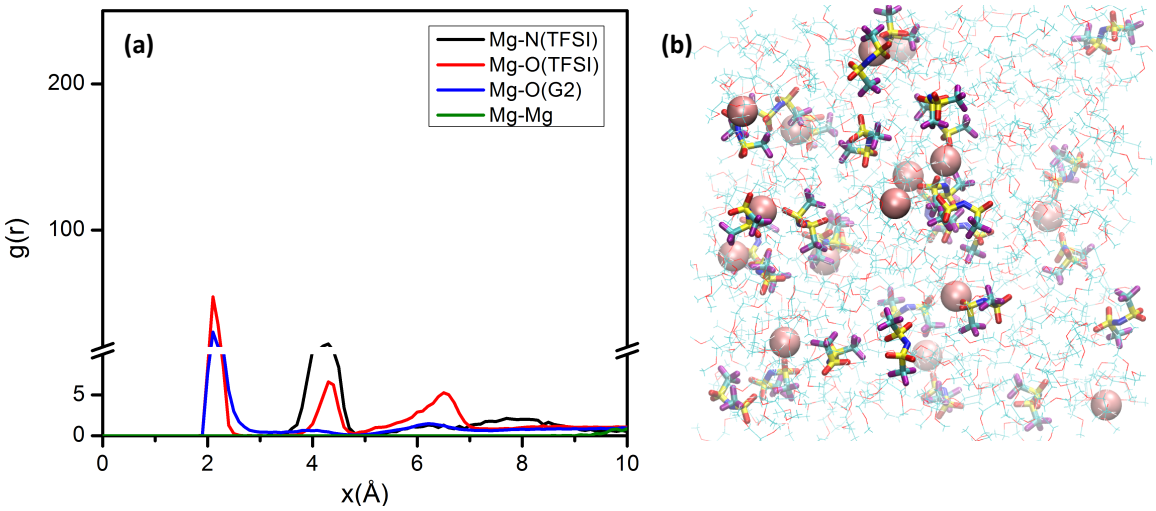


Figure S4. (a) Radial distribution function of Mg-N(TFSI), Mg-O(TFSI), Mg-O(G2) and Mg-Mg (b) representative simulation snapshot of 0.4 M $Mg(TFSI)_2$ in G2 at 298 K. Mg depicted in pink in space-filling format, TFSI in licorice and AN in line format

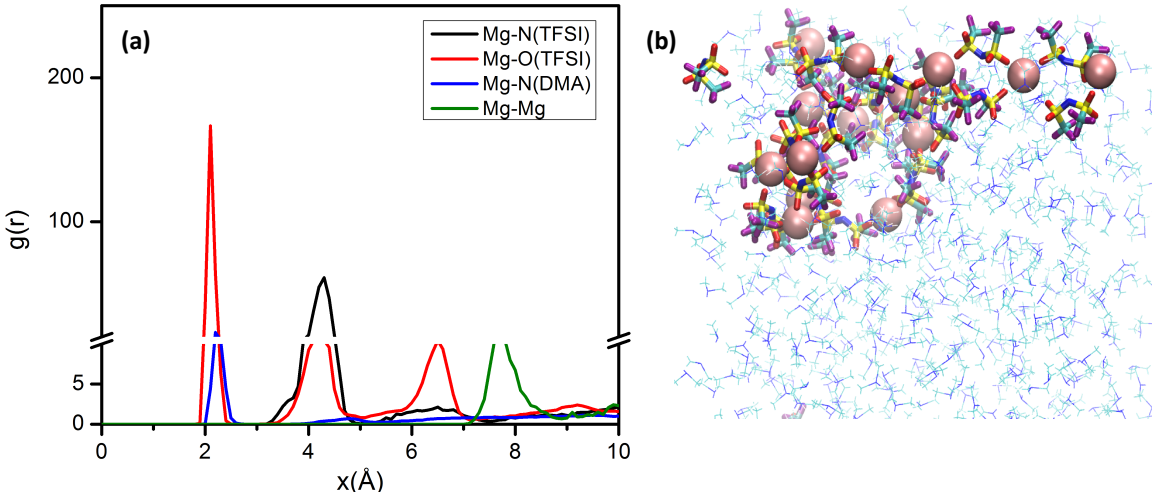


Figure S5. (a) Radial distribution function of Mg-N(TFSI), Mg-O(TFSI), Mg-N(DMA) and Mg-Mg(b) representative simulation snapshot of 0.4 M $Mg(TFSI)_2$ in DMA at 298 K. Mg depicted in pink in space-filling format, TFSI in licorice and AN in line format

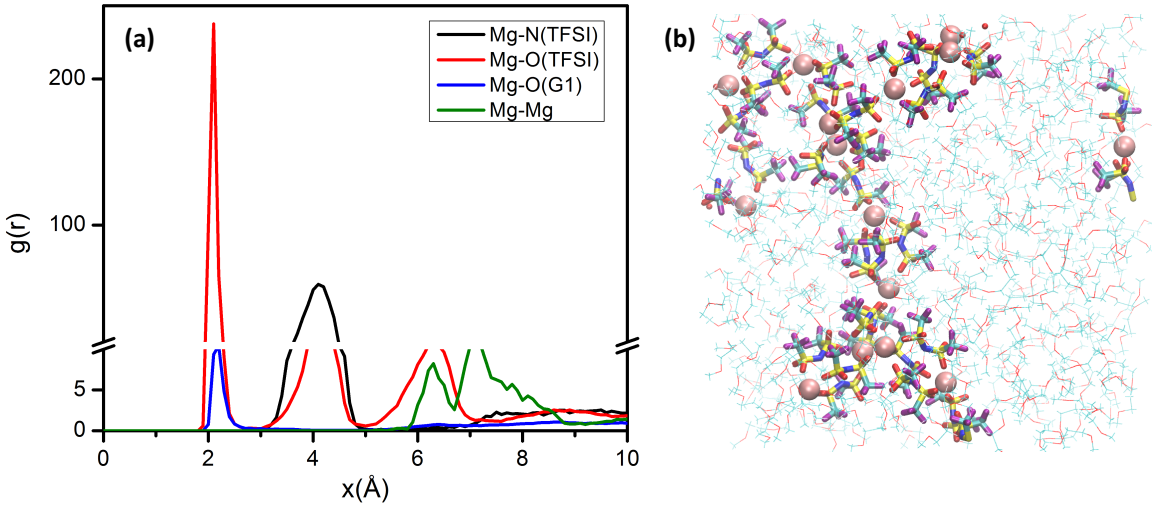


Figure S6. (a) Radial distribution function of Mg-N(TFSI), Mg-O(TFSI), Mg-O(G1) and Mg-Mg(b) representative simulation snapshot of 0.4 M $Mg(TFSI)_2$ in G1 at 298 K. Mg depicted in pink in space-filling format, TFSI in licorice and AN in line format

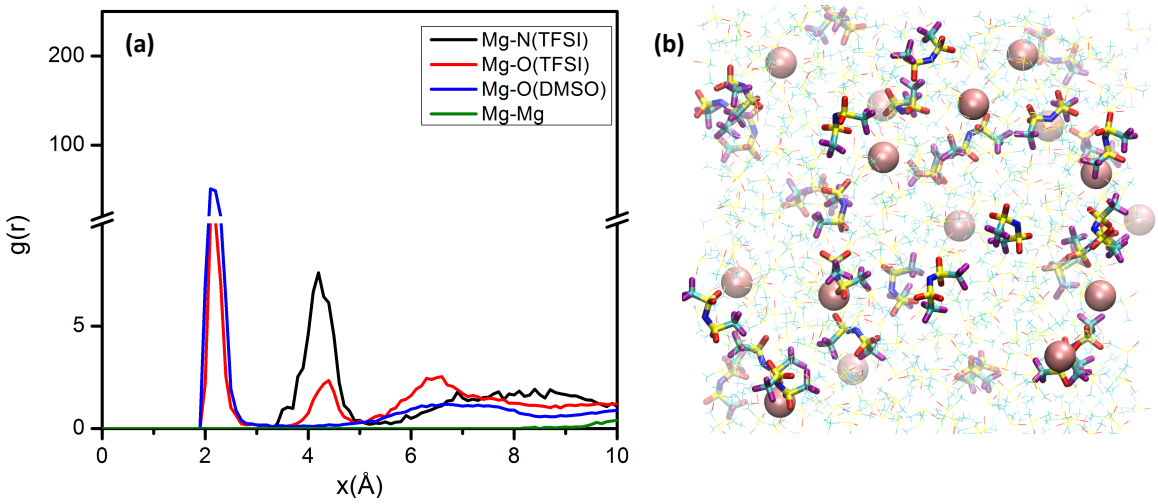


Figure S7. (a) Radial distribution function of Mg-N(TFSI), Mg-O(TFSI), Mg-O(DMSO) and Mg-Mg(b) representative simulation snapshot of 0.4 M $Mg(TFSI)_2$ in DMSO at 298 K. Mg depicted in pink in space-filling format, TFSI in licorice and AN in line format

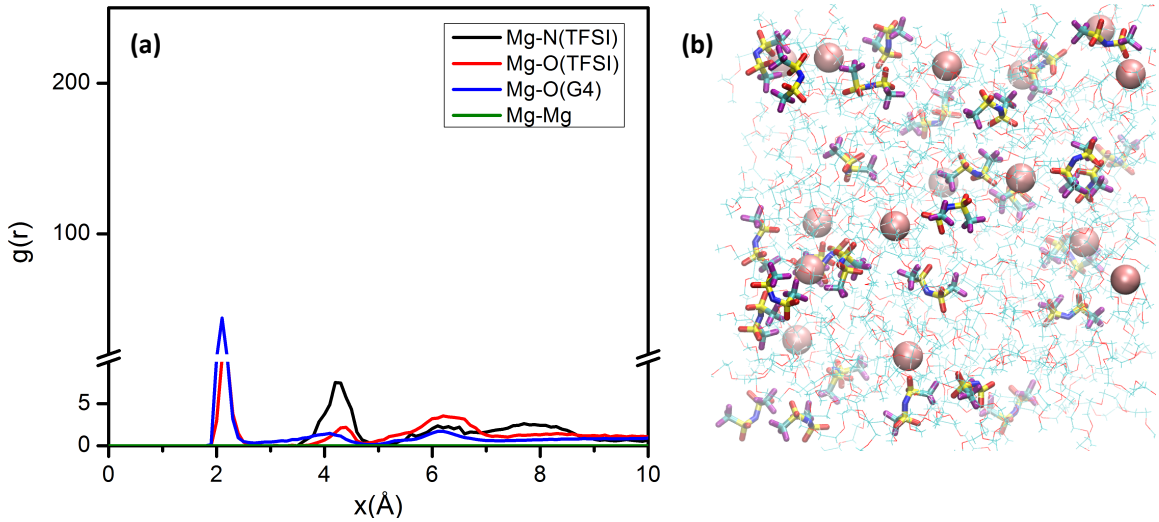


Figure S8. (a) Radial distribution function of Mg-N(TFSI), Mg-O(TFSI), Mg-O(G4) and Mg-Mg(b) representative simulation snapshot of 0.4 M $Mg(TFSI)_2$ in G4 at 298 K. Mg depicted in pink in space-filling format, TFSI in licorice and AN in line format

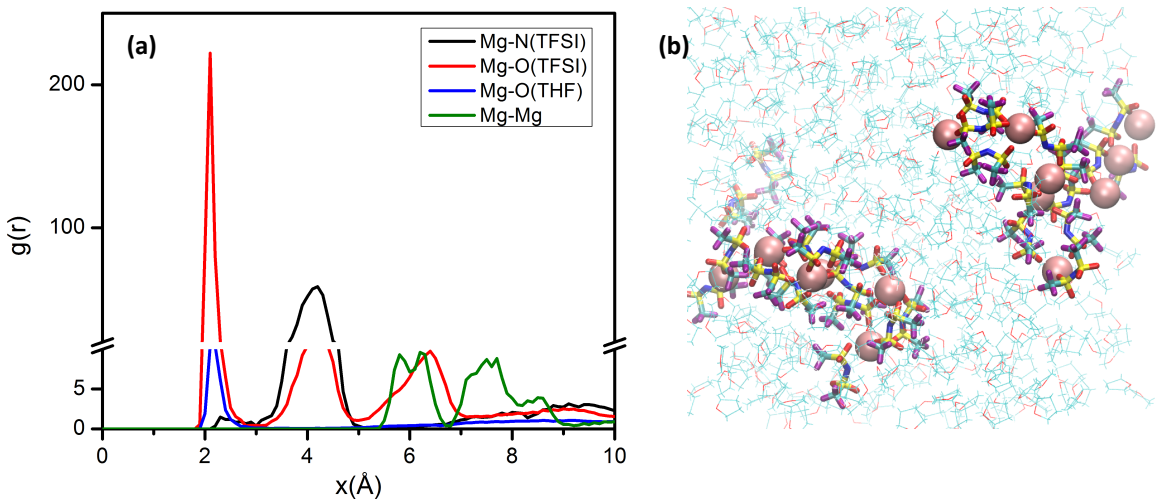


Figure S9. (a) Radial distribution function of Mg-N(TFSI), Mg-O(TFSI), Mg-O(THF) and Mg-Mg(b) representative simulation snapshot of 0.4 M $Mg(TFSI)_2$ in THF at 298 K. Mg depicted in pink in space-filling format, TFSI in licorice and AN in line format

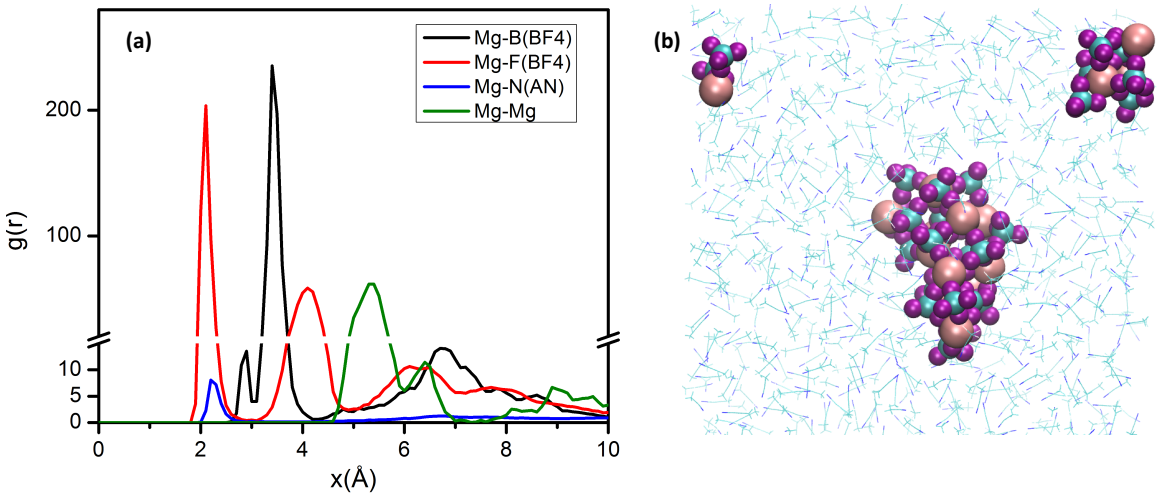


Figure S10. (a) Radial distribution function of Mg-B($BF_4$), Mg-F($BF_4$), Mg-N(AN) and Mg-Mg (b) representative simulation snapshot of 0.4 M $Mg(BF_4)_2$ in AN at 298 K. Mg, B and H are depicted in pink, green and magenta respectively in space-filling format. AN in line format

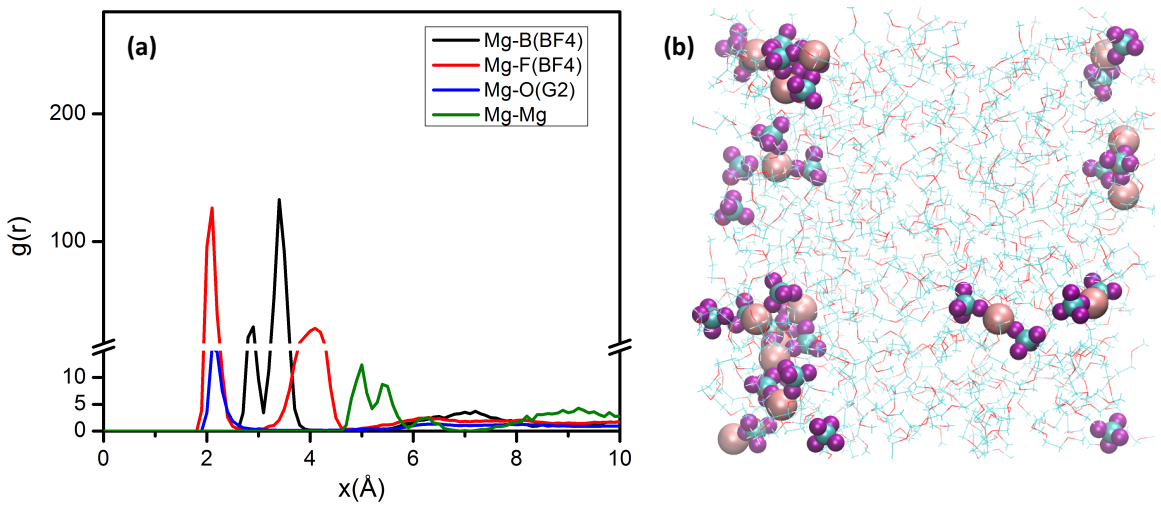


Figure S11. (a) Radial distribution function of Mg-B($BF_4$), Mg-F($BF_4$), Mg-O(G2) and Mg-Mg (b) representative simulation snapshot of 0.4 M $Mg(BF_4)_2$ in G2 at 298 K. Mg, B and H are depicted in pink, green and magenta respectively in space-filling format. G2 in line format

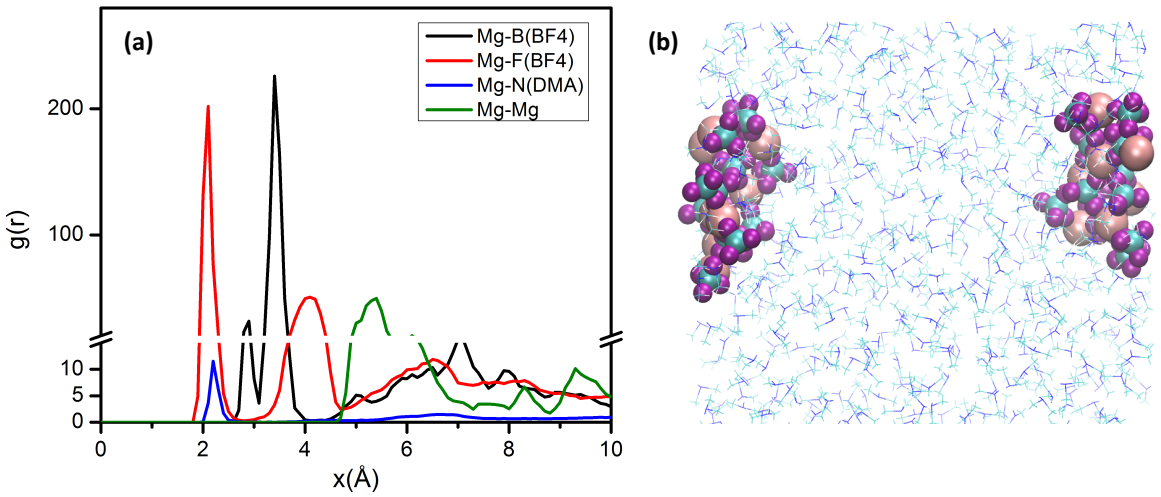


Figure S12. (a) Radial distribution function of Mg-B($BF_4$), Mg-F($BF_4$), Mg-N(DMA) and Mg-Mg(b) representative simulation snapshot of 0.4 M $Mg(BF_4)_2$ in DMA at 298 K. Mg, B and H are depicted in pink, green and magenta respectively in space-filling format. DMA in line format

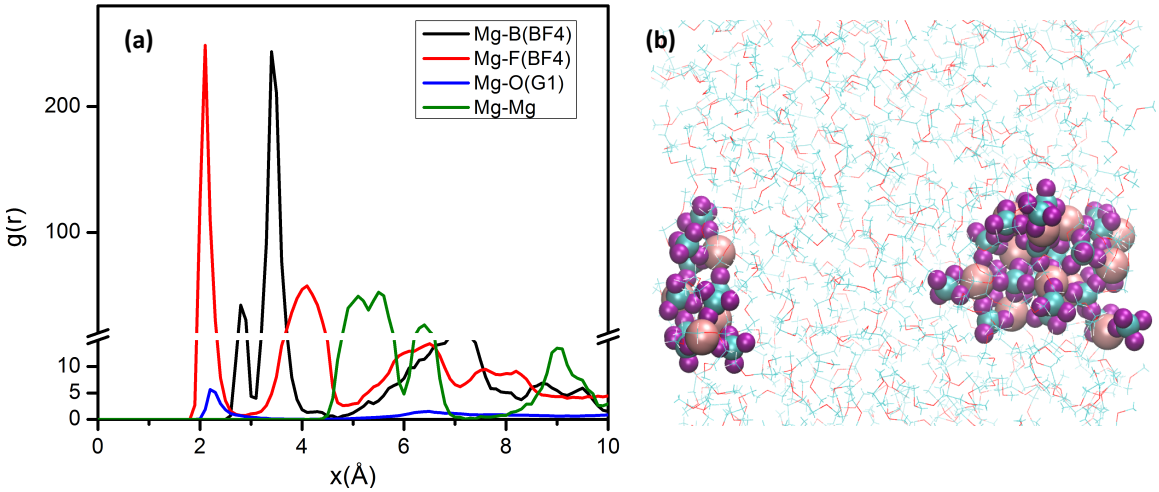


Figure S13. (a) Radial distribution function of Mg-B($BF_4$), Mg-F($BF_4$), Mg-O(G1) and Mg-Mg (b) representative simulation snapshot of 0.4 M $Mg(BF_4)_2$ in G1 at 298 K. Mg, B and H are depicted in pink, green and magenta respectively in space-filling format. G1 in line format

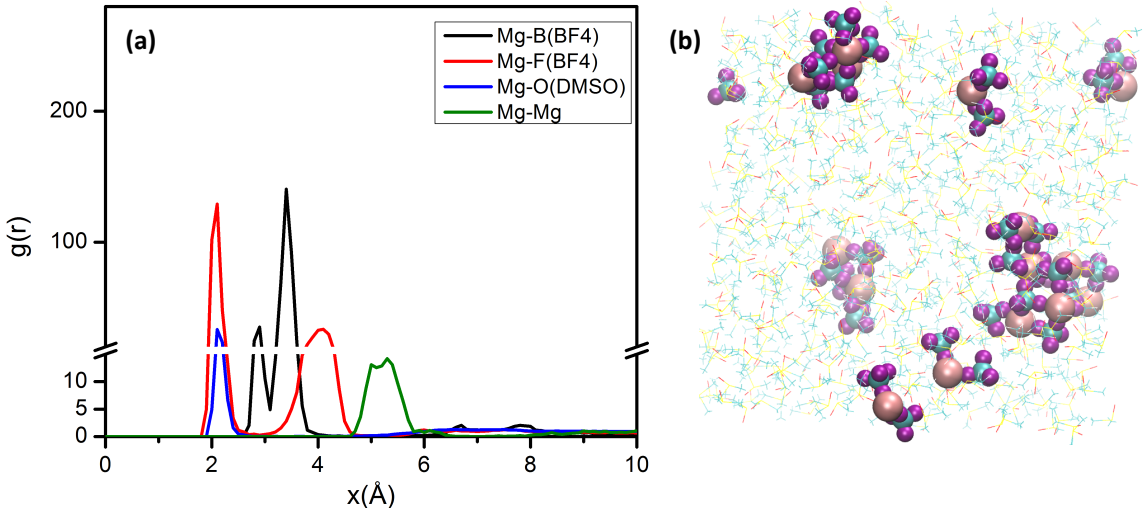


Figure S14. (a) Radial distribution function of Mg-B($BF_4$), Mg-F($BF_4$), Mg-O(DMSO) and Mg-Mg (b) representative simulation snapshot of 0.4 M $Mg(BF_4)_2$ in DMSO at 298 K. Mg, B and H are depicted in pink, green and magenta respectively in space-filling format. DMSO in line format

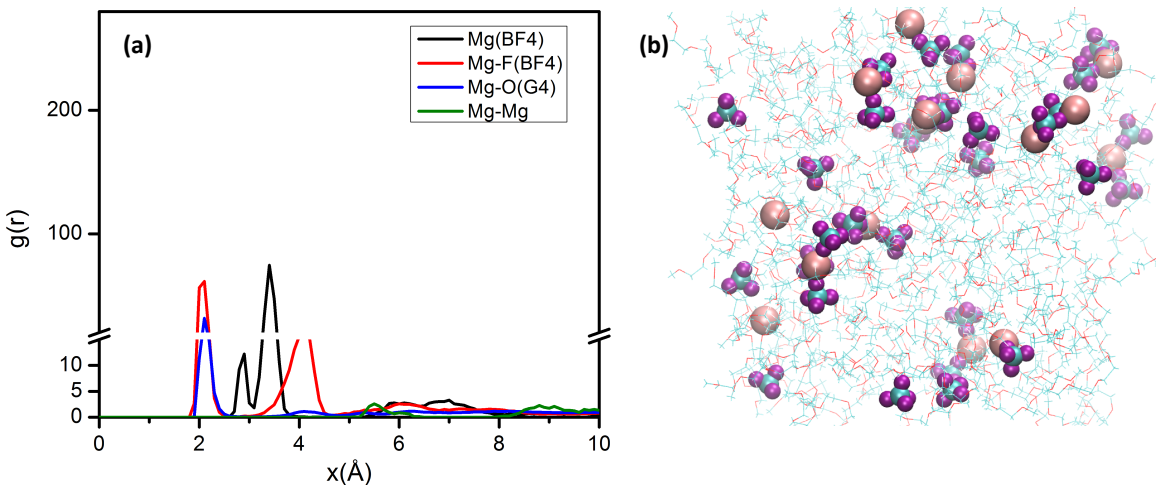


Figure S15. (a) Radial distribution function of Mg-B($BF_4$), Mg-F($BF_4$), Mg-O(G4) and Mg-Mg (b) representative simulation snapshot of 0.4 M $Mg(BF_4)_2$ in G4 at 298 K. Mg, B and H are depicted in pink, green and magneta respectively in space-filling format. G4 in line format

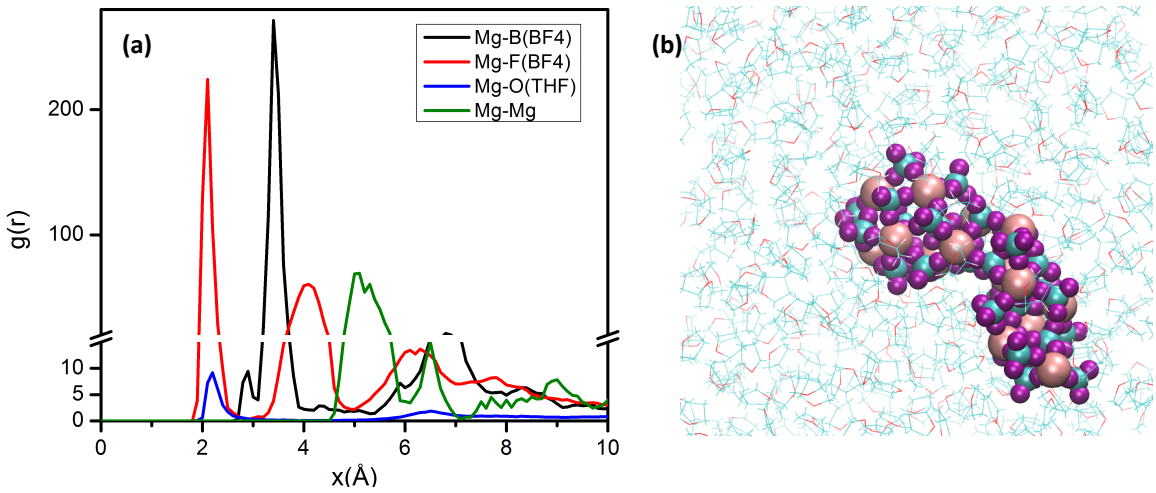


Figure S16. (a) Radial distribution function of Mg-B($BF_4$), Mg-F($BF_4$), Mg-O(THF) and Mg-Mg (b) representative simulation snapshot of 0.4 M $Mg(BF_4)_2$ in THF at 298 K. Mg, B and H are depicted in pink, green and magneta respectively in space-filling format. THF in line format

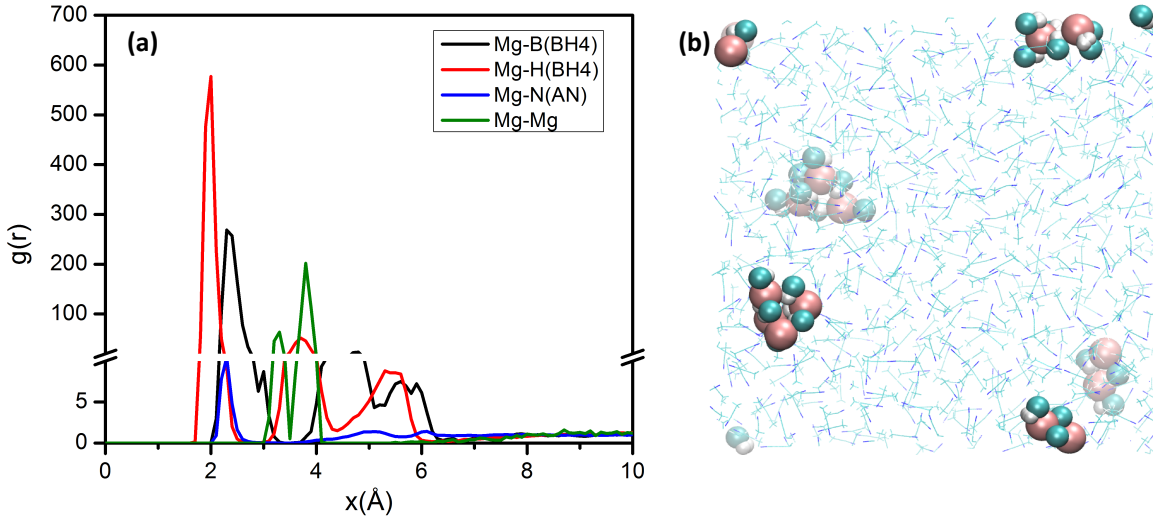


Figure S17. (a) Radial distribution function of Mg-B($BH_4$), Mg-H($BH_4$), Mg-N(AN) and Mg-Mg (b) representative simulation snapshot of 0.4 M $Mg(BH_4)_2$ in AN at 298 K. Mg, B and H are depicted in pink, green and magneta respectively in space-filling format. AN in line format

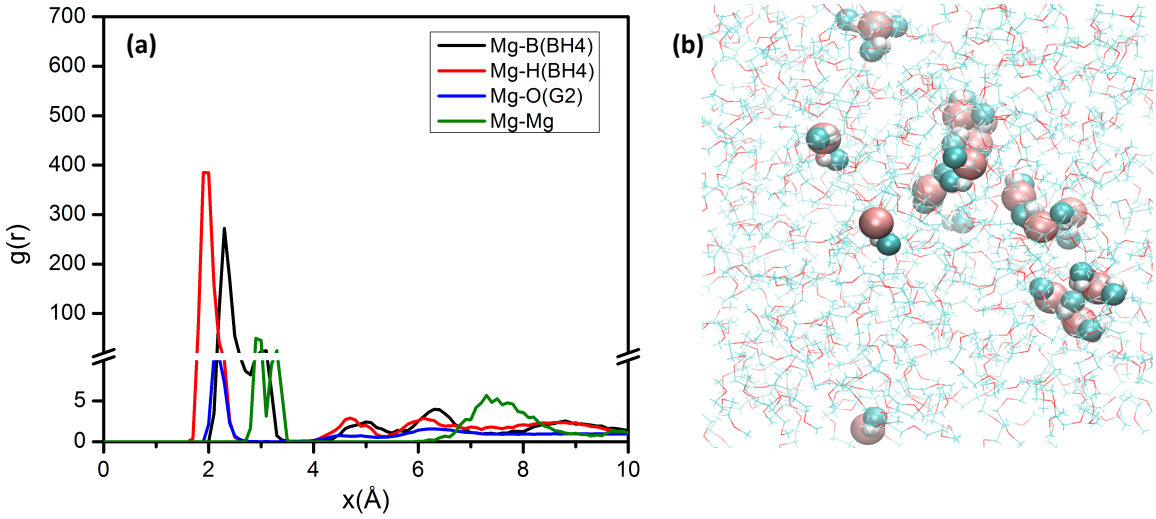


Figure S18. (a) Radial distribution function of Mg-B($BH_4$), Mg-H($BH_4$), Mg-O(G2) and Mg-Mg (b) representative simulation snapshot of 0.4 M $Mg(BH_4)_2$ in G2 at 298 K. Mg, B and H are depicted in pink, green and magenta respectively in space-filling format. G2 in line format

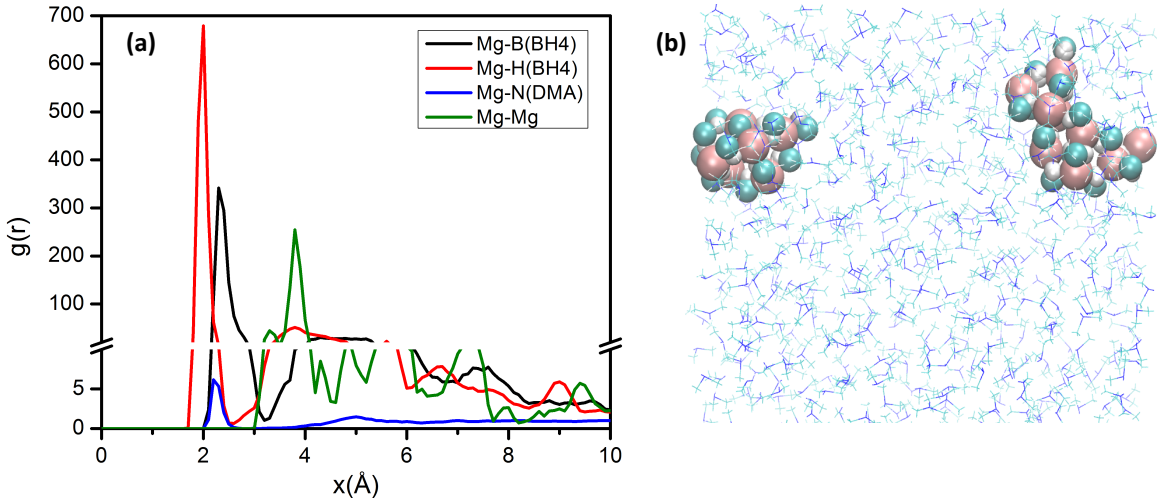


Figure S19. (a) Radial distribution function of Mg-B($BH_4$), Mg-H($BH_4$), Mg-N(DMA) and Mg-Mg (b) representative simulation snapshot of 0.4 M $Mg(BH_4)_2$ in DMA at 298 K. Mg, B and H are depicted in pink, green and magenta respectively in space-filling format. DMA in line format

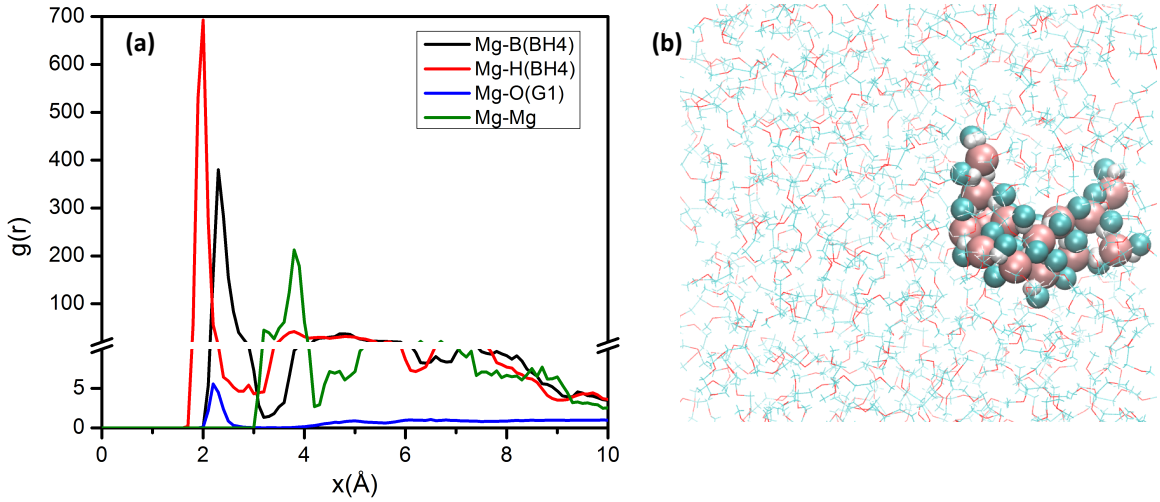


Figure S20. (a) Radial distribution function of Mg-B($BH_4$), Mg-H($BH_4$), Mg-O(G1) and Mg-Mg (b) representative simulation snapshot of 0.4 M $Mg(BH_4)_2$ in G1 at 298 K. Mg, B and H are depicted in pink, green and magenta respectively in space-filling format. G1 in line format

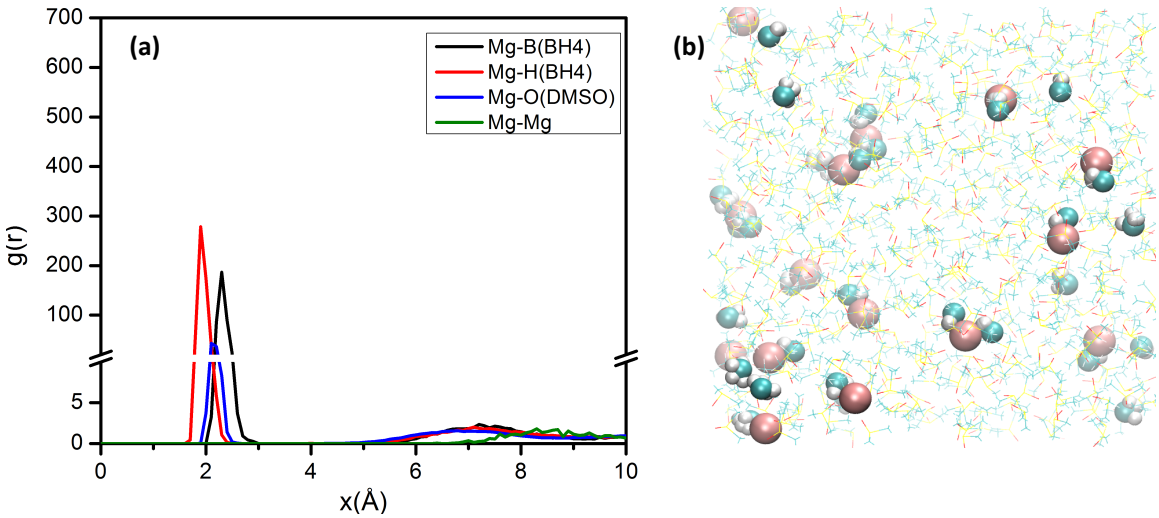


Figure S21. (a) Radial distribution function of Mg-B($BH_4$), Mg-H($BH_4$), Mg-O(DMSO) and Mg-Mg (b) representative simulation snapshot of 0.4 M $Mg(BH_4)_2$ in DMSO at 298 K. Mg, B and H are depicted in pink, green and magenta respectively in space-filling format. DMSO in line format

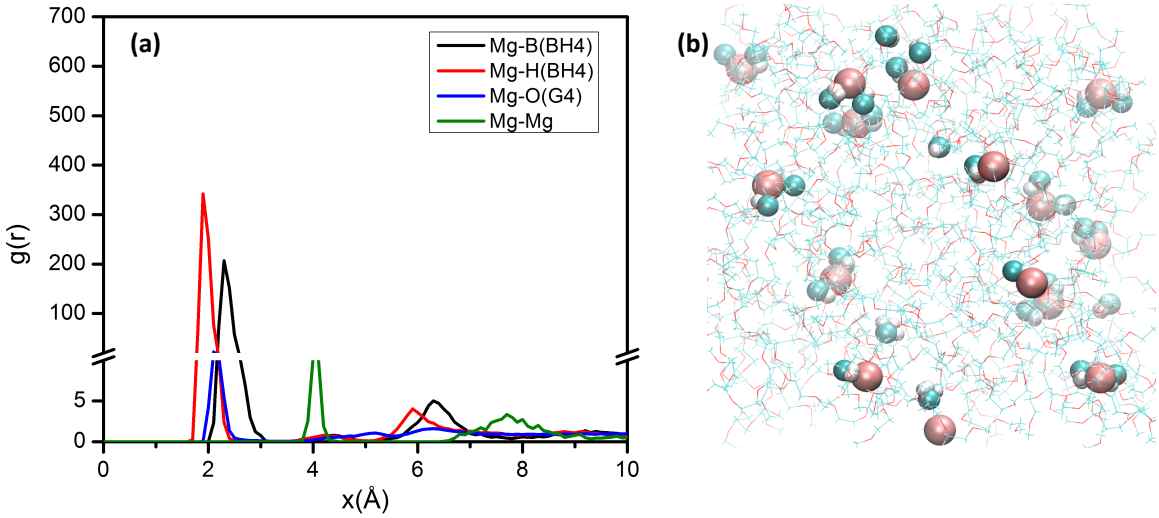


Figure S22. (a) Radial distribution function of Mg-B($BH_4$), Mg-H($BH_4$), Mg-O(G4) and Mg-Mg (b) representative simulation snapshot of 0.4 M $Mg(BH_4)_2$ in G4 at 298 K. Mg, B and H are depicted in pink, green and magenta respectively in space-filling format. G4 in line format

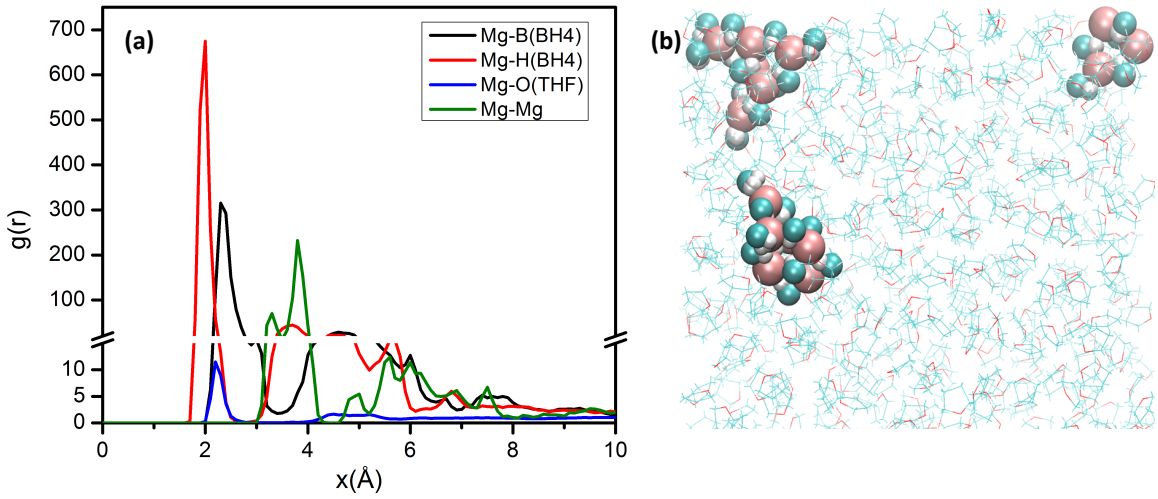


Figure S23. (a) Radial distribution function of Mg-B($BH_4$), Mg-H($BH_4$), Mg-O(THF) and Mg-Mg (b) representative simulation snapshot of 0.4 M $Mg(BH_4)_2$ in THF at 298 K. Mg, B and H are depicted in pink, green and magenta respectively in space-filling format. THF in line format

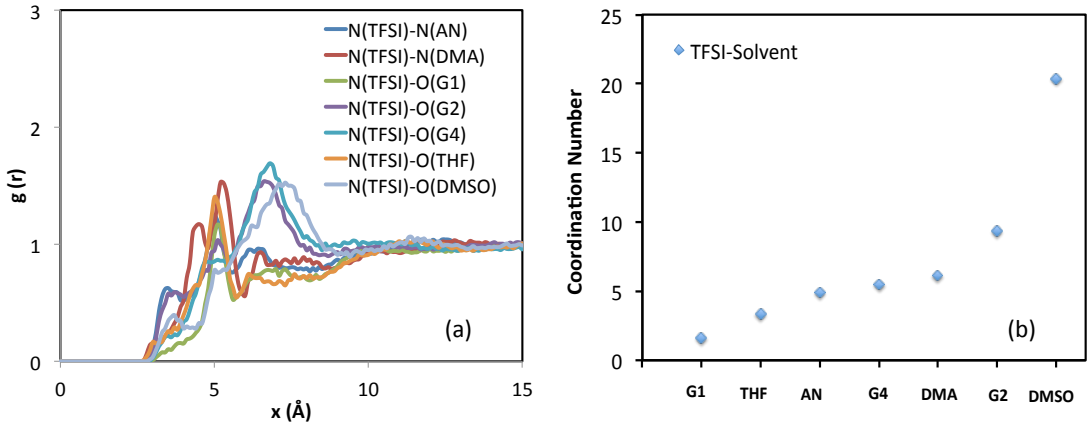


Figure S24. (a) Radial distribution function of N(TFSI)-N(AN), N(TFSI)-N(DMA), N(TFSI)-O(G1), N(TFSI)-O(G2), N(TFSI)-O(G4), N(TFSI)-O(THF), N(TFSI)-O(DMSO) (b) Coordination Number of TFSI-AN, TFSI-DMA, TFSI-G1, TFSI-G2, TFSI-G4, TFSI-THF, TFSI-DMSO computed by integrating the first peak of N(TFSI)-N(AN), N(TFSI)-N(DMA), N(TFSI)-O(G1), N(TFSI)-O(G2), N(TFSI)-O(G4), N(TFSI)-O(THF), N(TFSI)-O(DMSO) respectively.

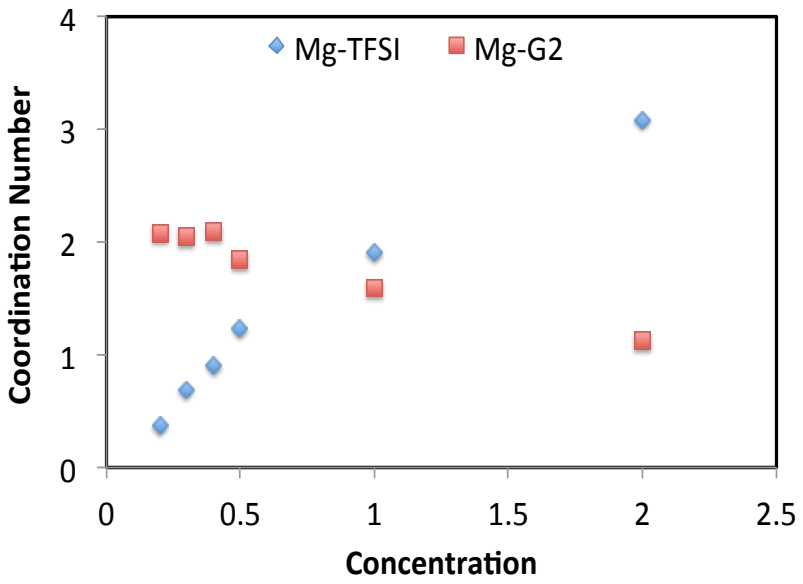


Figure S25. Coordination number of Mg-TFSI and Mg-G2 in $Mg(TFSI)_2$/G2 solution as a function of concentration calculated from MD simulations

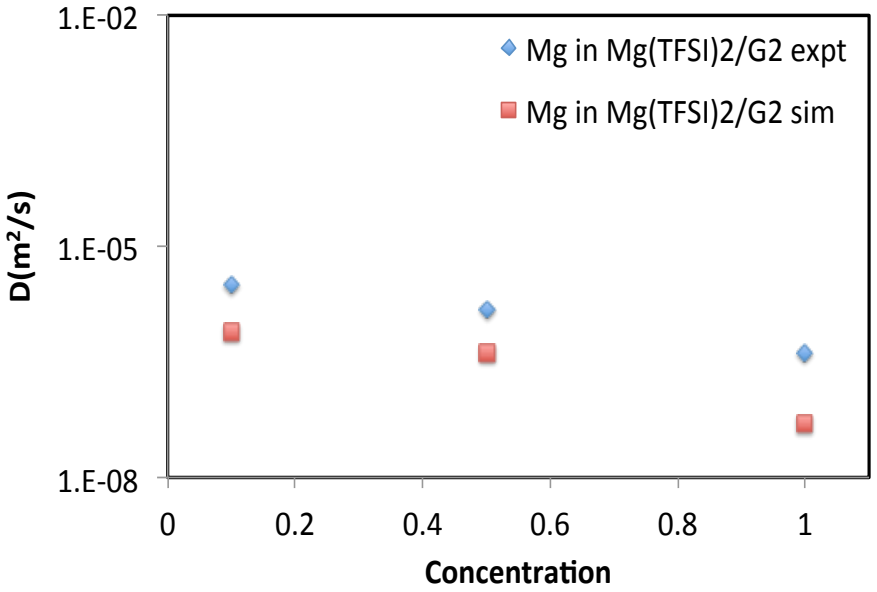


Figure S26. Diffusion coefficient of Mg in $Mg(TFSI)_2$/G2 as a function of concentration from MD simulations and chronocoulometry method

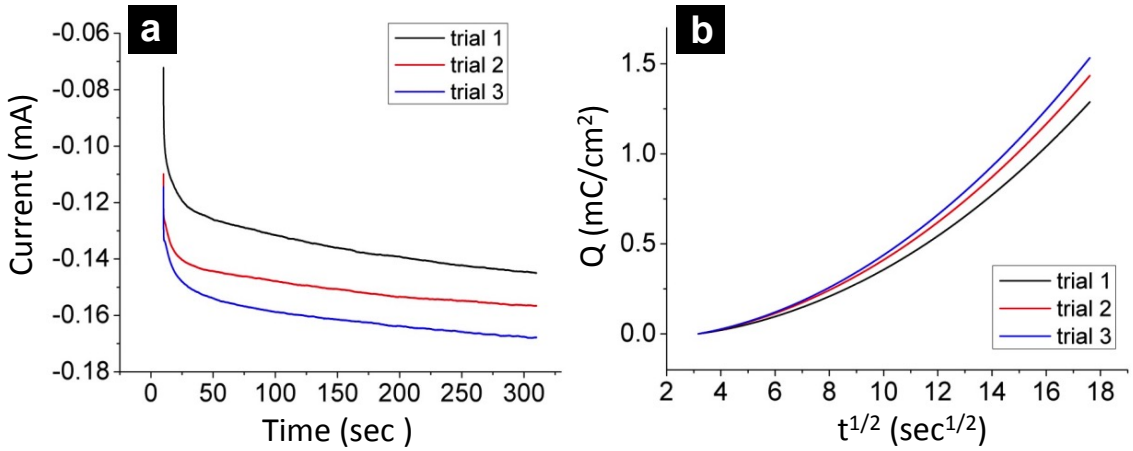


Figure S27. (a). Chronocoulometry (CC) curves of 0.4 M $Mg(TFSI)_2$ in diglyme for three trials. A three-electrode setup is used, with Pt disk as working electrode and Mg ribbon as counter and reference electrode. Potential at Pt disk is held at -0.5 V. (b). Anson plot of 0.4 M $Mg(TFSI)_2$ in G2 for three trials.

References


(1) Ha, S.-Y.; Lee, Y.-W.; Woo, S. W.; Koo, B.; Kim, J.-S.; Cho, J.; Lee, K. T.; Choi, N.-S. *ACS Applied Materials & Interfaces* **2014**, *6*, 4063.

(2) Mohtadi, R.; Matsui, M.; Arthur, T. S.; Hwang, S.-J. *Angewandte Chemie International Edition* **2012**, *51*, 9780.

(3) Shao, Y.; Liu, T.; Li, G.; Gu, M.; Nie, Z.; Engelhard, M.; Xiao, J.; Lv, D.; Wang, C.; Zhang, J.-G. *Scientific reports* **2013**, *3*.

(4) Ue, M.; Takeda, M.; Takehara, M.; Mori, S. *Journal of the Electrochemical Society* **1997**, *144*, 2684.

(5) Wu, X.; Liu, Z.; Huang, S.; Wang, W. *Physical Chemistry Chemical Physics* **2005**, *7*, 2771.

(6) Aminabhavi, T. M.; Gopalakrishna, B. *Journal of Chemical & Engineering Data* **1995**, *40*, 856.

(7) Hayamizu, K.; Aihara, Y.; Arai, S.; Garcia *The Journal of Physical Chemistry B* **1999**, *103*, 519.

(8) Packer, K.; Tomlinson, D. *Transactions of the Faraday Society* **1971**, *67*, 1302.

(9) Lago, A.; Rivas, M. A.; Legido, J.; Iglesias, T. P. *The Journal of Chemical Thermodynamics* **2009**, *41*, 257.

(10) Rivas, M. A.; Iglesias, T. P.; Pereira, S. M.; Banerji, N. *The Journal of Chemical Thermodynamics* **2006**, *38*, 245.

(11)http://www2.dupont.com/Methylamines/en_US/tech_info/index.html).

(12) Guevara-Carrion, G.; Vrabec, J.; Hasse, H. *Fluid Phase Equilibria* **2012**, *316*, 46.